COLLEGIATE WIND COMPETITION
U.S. DEPARTMENT OF ENERGY

Team and Electrical Lead:
Kitt Connor

Electrical Engineers:
Mohammad Aldaihani
Shreya Timilsina

Mechanical Lead:
Daylon Black

Mechanical Engineers:
Anthony Gianforcaro
Jason Kuwada
Kevin Barreto

Professors and Mentors:
Brian Higgins - Electrical
Chris Davis
Lynn Catlin - Mechanical

Contents

Executive Summary:

The Boise State University College of engineering set up a team of seven engineers to design, build and test an aerodynamically, mechanically and electrically efficient wind turbine to compete in the Collegiate Wind Competition in Boulder Colorado in 2017. This team, consisting of four mechanical engineers and three electrical engineers produced a turbine that can yaw which will yield power generation in any wind direction. Using a stepper motor and a rotary encoder the turbine is able to sense the wind direction and turn into the wind. Variable pitch was a necessity for the braking system as large capacitors were not allowed. This was accomplished using a stepper motor and a spring on a rack and pinion system. This will make sure the blades are always feathered until the stepper motor is activated. This will ensure that the system can break when the load is disconnected. The load designed is a water cooling system used to cool the electronics of the turbine. This was accomplished using a water pump connected to water blocks that will be attached to the electronics that generate a lot amount of heat. The flowing fluid will then draw the heat away from the components keeping them from overheating.

Technical Design:

This year the team focused on creating a turbine that could operate within a range of wind speeds between 5 and 18 meters per second, have a constant power output, have a low cut in speed, be able to yaw into the wind and have working variable pitch blades.

The mechanical design of the wind turbine was broken up into three main design components, blades, variable pitch, and yaw system. The blade design was quantified using blade element and momentum theory and cross sectional area of common airfoil profiles in order to achieve the strongest and most efficient blade design for the turbine. The variable pitch component was designed to produce a low cut-in speed, to maximize efficiency of the power to wind speed ratio, and finally to achieve a quick and efficient braking system. Lastly, the yaw system was designed to locate the wind and then rotate the turbine in order to maintain an angle perpendicular from the blades to the wind.

Rotor and Blades:

Blade design was calculated to include wake rotation of the rotor. Blade element and momentum theory was calculated using wake rotation of the rotors to provide three optimum blades, and can be seen in Table 1 (J. F. Manwell). Because of the nature of the competition, the design including a three-blade rotor with a tip speed ratio of six was chosen. In designing geometry of the blades, an angle of attack of zero was used. Angle of attack will be addressed using the variable pitch system of the turbine.

Table 1. Optimum Blade Design

r/R	$\lambda = 1$ $B = 1/2$		$\lambda = 6$ $B = 3$		$\lambda = 10$ $B = 2$	
	φ	c/R	φ	c/R	φ	c/R
0.95	31	0.284	6.6	0.053	4.0	0.029
0.85	33.1	0.289	7.4	0.059	4.5	0.033
0.75	35.4	0.291	8.4	0.067	5.1	0.037
0.65	37.9	0.288	9.6	0.076	5.8	0.042
0.55	40.8	0.280	11.2	0.088	6.9	0.050
0.45	43.8	0.263	13.5	0.105	8.4	0.060
0.35	47.1	0.234	17.0	0.128	10.6	0.075
0.25	50.6	0.192	22.5	0.159	14.5	0.100
0.15	54.3	0.131	32.0	0.191	22.5	0.143
Solidity, σ		0.86		0.088		0.036

Note: B, number of blades; c, airfoil chord length; r, blade section radius; R, rotor radius; λ, tip speed ratio; φ, angle of relative wind

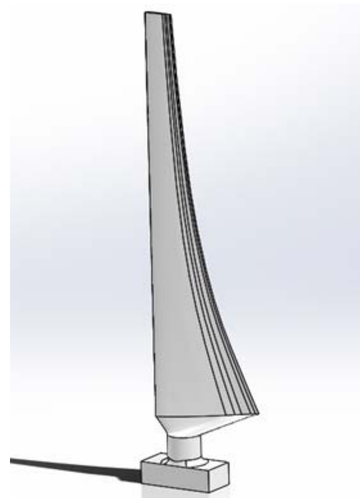

Figure 1. Sample Blade Design

With blade geometry completed, three different airfoils, (NACA-0012, NACA 64-215, LS(1)-417), were propagated through the blade as cross sectional areas. The three airfoils are commonly used in wind turbine blade applications and have varying thicknesses and cambers. The connection of the blade to the variable pitch system is modeled to be compatible with previous year's designs, this allows for redundancies and the opportunity to use the previous turbine for a baseline in testing.

Three blade design were designed and created in 3D CAD modeling; blades differed in cross sectional areas. A flow analysis was done on SOLIDWORKS, using a wind speed of 10 m/s and an angle of attack of zero degrees. A pressure gradient was simulated from given conditions and can be seen in Figure 2

A summary table of the results can be found on Table 2. The blade designed using the airfoil LS(1)-417

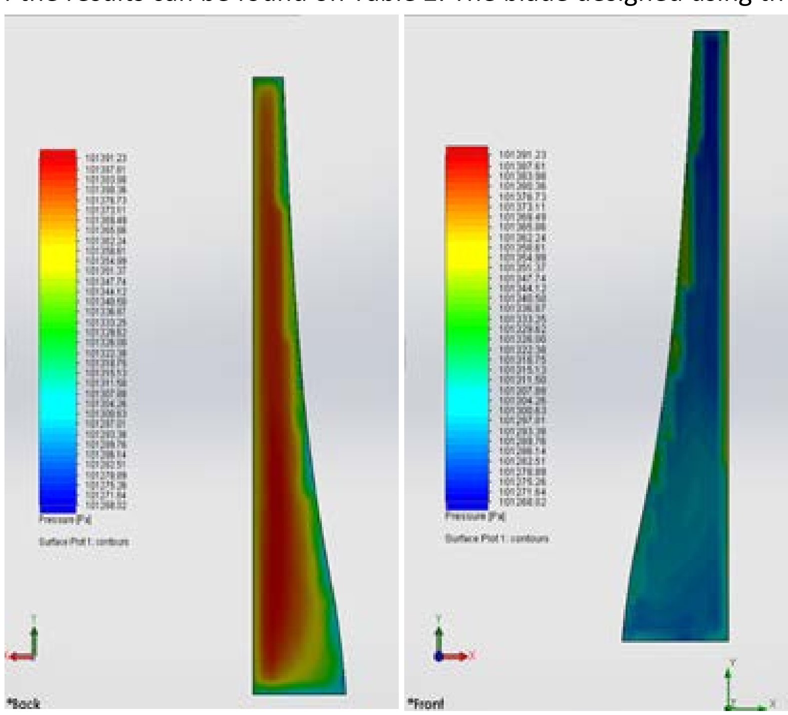

Figure 2. Sample Flow Analysis

was chosen because showed a slightly larger value for the difference of pressure as well as being a more aggressive blade design.

Table 2. Blade Flow Analysis Summary

Air Foil	Goal Name	Unit	Value	Averaged Value	Minimum Value	Maximum Value	Delta
NACA0012	SG Av Static Pressure 1	[Pa]	101328.00	101327.94	101327.41	101329.13	1.72
	SG Normal Force 1	[N]	0.28	0.28	0.27	0.28	0.01
NACA64215	SG Av Static Pressure 1	[Pa]	101327.95	101327.76	101327.41	101328.12	0.71
	SG Normal Force 1	[N]	0.30	0.31	0.30	0.31	0.01
LS417	SG Av Static Pressure 1	[Pa]	101328.08	101328.06	101327.65	101329.50	1.85
	SG Normal Force 1	[N]	0.30	0.30	0.28	0.30	0.02

To evaluate performance of the blades, blade element and momentum theory was reapplied to the designed blade, with the use of empirical data. Angular and axial induction factors were calculated using an iterative solution to solve for optimum angle of relative wind, as well as, coefficients of thrust and lift. By taking the preexisting measurements of section pitch, solved by (NASA), and calculated values of angle of relative wind, at differing tip speed ratios, optimum angle of attack was found for each tip speed ratio. Using the optimum angles of attack, a Cp vs Lambda curve was created, and can be seen in Figure 3. A summary table of angle of attack and corresponding power coefficient can be seen in Table 3.

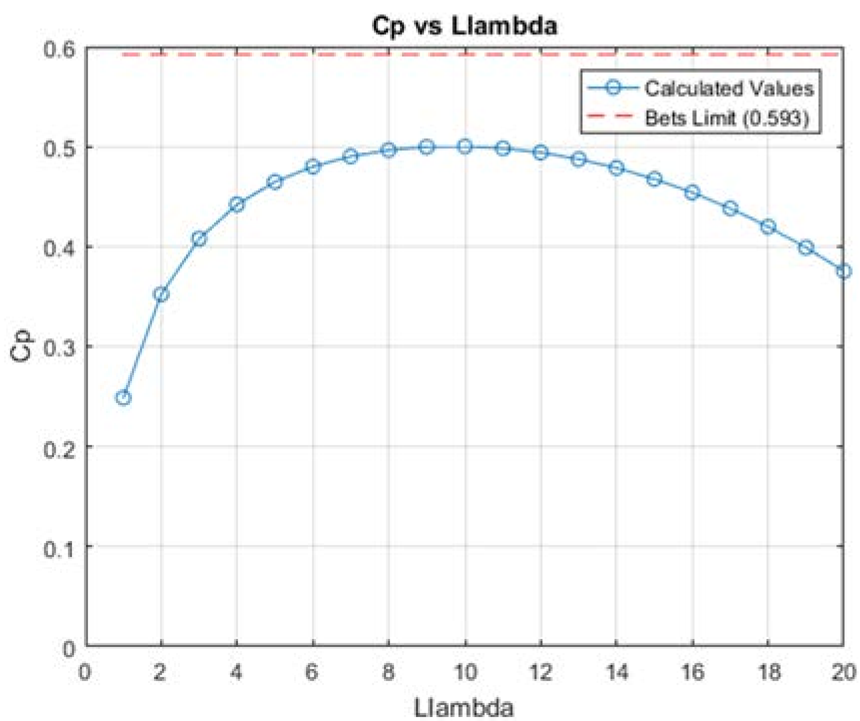

Figure 3. Cp vs Lambda

Table 3. Angle of Attack

Tip Speed Ratio	Power Coefficient	Angle of Attack (Degrees)
1	0.2490	41.68
2	0.3520	24.12
3	0.4078	14.58
4	0.4421	8.69
5	0.4647	4.73
6	0.4800	1.90
7	0.4901	-0.22
8	0.4965	-1.85
9	0.4997	-3.16
10	0.5002	-4.21

Tip Speed Ratio	Power Coefficient	Angle of Attack (Degrees)
11	0.4983	-5.09
12	0.4940	-5.83
13	0.4874	-6.46
14	0.4786	-7.00
15	0.4675	-7.47
16	0.4540	-7.88
17	0.4382	-8.25
18	0.4198	-8.58
19	0.3989	-8.87
20	0.3753	-9.14

A stress analysis of the designed blades was completed on major stresses, (gravity, yaw, and centrifugal effects), as they propagate through the blade. Calculations were done using 10 elements and a rectangular approximation for the cross-sectional areas. Stresses plotted against rotor radius can be seen in Figure 4, and calculations can be seen in Appendix I – Matlab Calculations:.

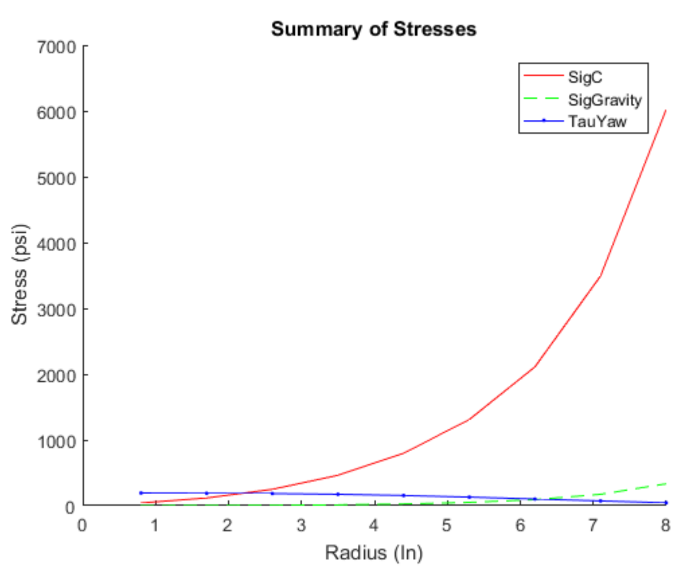

Figure 4. Stress Analysis

Variable Pitch:

The variable pitch system of the turbine can be broken down into two subsystems, the nose and the nacelle of the turbine. The nose system shown in Figure 5 was designed to be lightweight and durable. The nose hub and nose cone of the turbine for weight purposes were 3-D printed using Polylactide (PLA) filament which has a tensile strength of about 56 MPa. The blade rotational caps were also 3-D printed and were designed to hold the brass bushings in place. These bushings help to allow rotation of the blades while simultaneously supporting the estimated 70 N centripetal force. The variable pitch shaft that moves linearly, was connected to the nose cap through a simple yet effective assembly. The nose cap contains an internal press fitted bearing rated for a max rpm of 50,000 which the turbine will only achieve an estimated 3,000 rpm. Two thrust bearings enclose the nose cap on both sides rated with a dynamic load of about 215 N whereas the turbine is only expected to see 22 N. The blades are connected to the nose cap by lever arms that have a brass bushing on one side. The brass bushing is attached to the side that will rotated about 90 degrees and not on the side that will rotate about 23 degrees. This assembly was designed with the intent of the nose cap to rotate and not the variable pitch shaft.

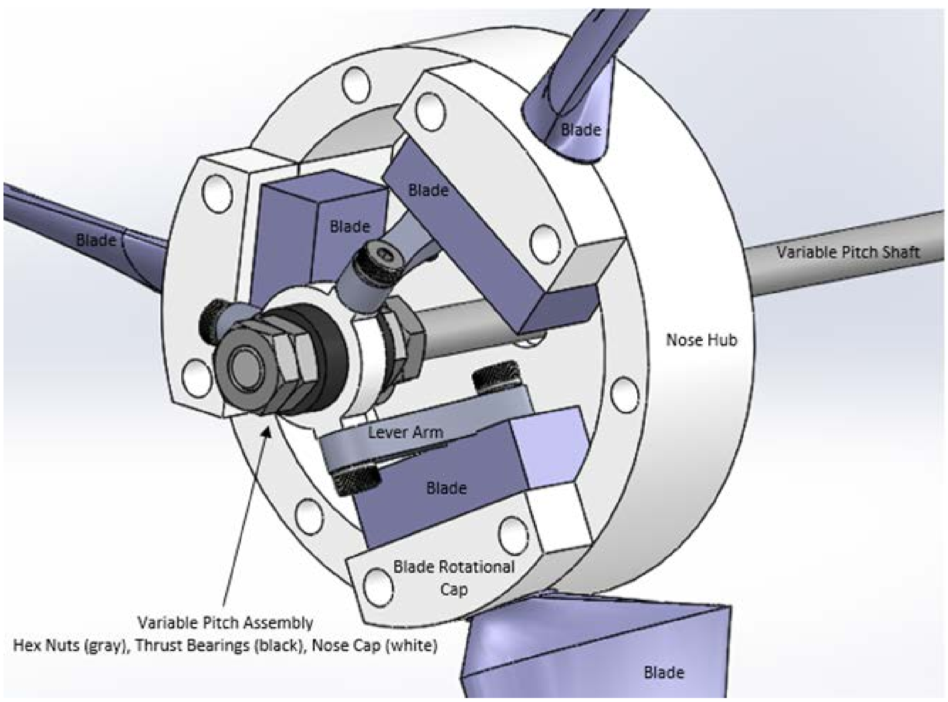

Figure 5. Variable Pitch Nose Assembly

The second subsystem of the turbine, the nacelle shown in Figure 6, was broken down into three components, variable pitch, power generation, and yaw. The variable pitch shaft is screwed into the variable pitch block which is mounted to the linear slides that allow for linear motion. The top of the variable pitch block is connected through a rack and pinion to the stepper motor that will rotate depending on the nose's rpm. The rack and pinion has a gear ratio of 1:1 and the stepper motor has a holding torque of 48 N*cm and a detent torque of 2.2 N*cm. This motor was chosen because the required torque will be no greater than 46 N*cm and the motor only requires three volts to power. This will allow for the pitch of the blades to be altered when power is available. When power is unavailable, shut down or catastrophic failure, the spring, having a spring constant of 5.5 lbs/in will overcome the detent torque and the blades will rotate to full feather, stopping the turbine almost immediately.

The power generation component of the nacelle revolved around a precision machined power shaft. The shaft was press fitted into the hub and the two ABEC 7 ceramic hybrid bearings, which have a max rpm of about 38,000 rpm. Using a tip speed ratio of 6 and a rotor diameter of about 46 cm, it was determined that the optimal wing tip velocity with an 11 m/s wind is 66 m/s, thus the target rotor speed of around 3000 RPM was used to calculate the gear ratio. With the desired operating voltage of 5V, and the generator manufacture recommendation of 1800 RPM/V, the ideal gear ratio was calculated to be 1:3. The gears purchased determined the final gear ratio to be about 1:3.1.

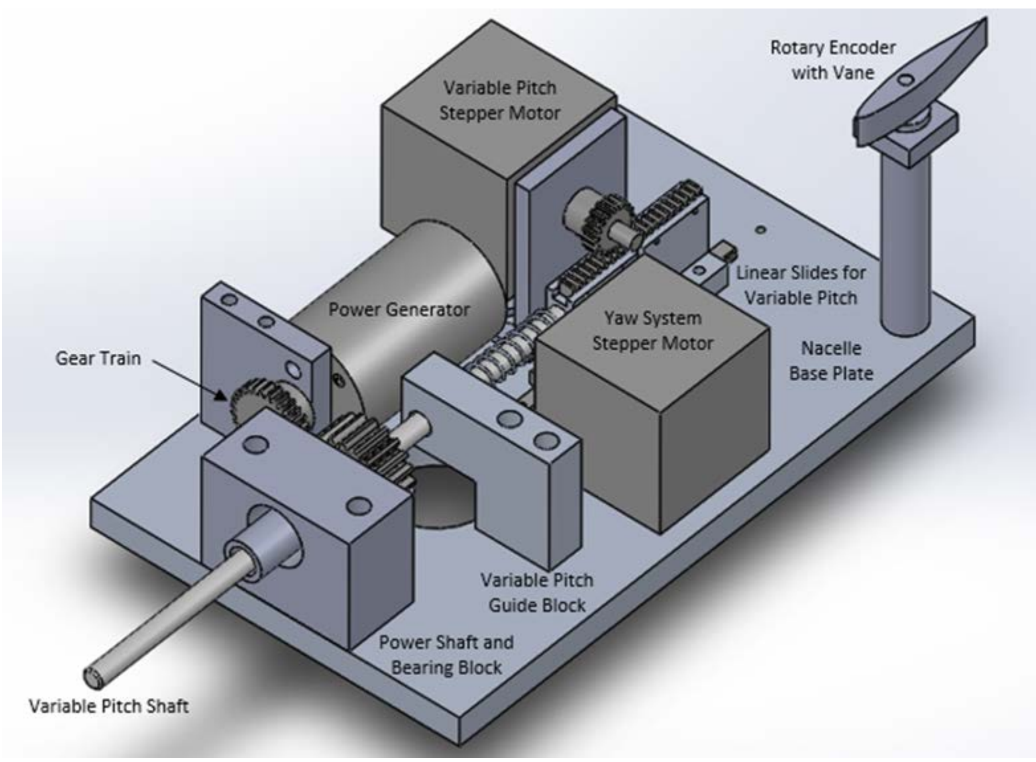

Figure 6. Variable Pitch Nacelle Assembly

Yaw System and Base Structure:

The Yaw system has a relatively simple mechanical design consisting of a shaft welded to the nacelle allowing the nacelle to rotate about an oil embedded bearing pressed and fixed on the tower. The yaw system functions through a stepper motor, which is mounted on the nacelle, that engages a gear fixed on the tower to produce the yaw. Figure 7 displays only the yaw and base structure components in a cross section view. Not shown in this figure are the rotary encoder and wind vane, shown in Figure 6, that signal to the electrical control board for the operation of the stepper motor. The signal and

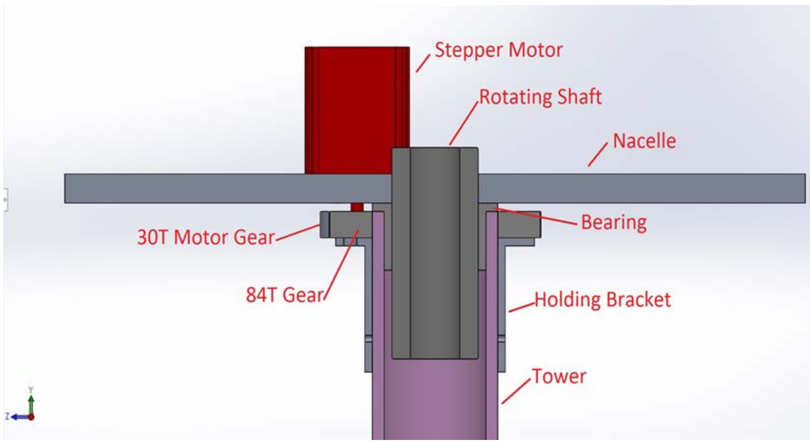

operation will be discussed in detail in a later section.

Figure 7. Yaw System

The yaw system needed to meet a certain specification. In specification F, the turbine must be capable of a maximum yaw rate of 180 degrees per second. In the designing of the yaw system one of the most important questions asked was how the yaw motion would be affected by the chosen motor and gear ratio. The answer to this question was in a force, dynamics and gear train analysis relating critical aspects that have an influence in yaw motion. The following equation is the result of the analysis.

$$\alpha_3 = -\frac{\tau}{r_1}\left[\frac{I_1}{r_1}\left(\frac{N_2}{N_1}+1\right) - \frac{I_3}{l} - m_1 r_1\left(\frac{N_2}{N_1}+1\right)\right]^{-1} \tag{1}$$

Where tau is the input motor torque, r_1 is the radius of the pitch circle of the motor gear, I_1 is the mass moment of inertia of the motor gear, N_2 is the teeth number of the sun gear, N_1 is the teeth number of the motor gear, I_3 is the mass moment of inertia of the nacelle, l is the center to center distance between the two gears, and m_1 is the mass of the motor gear. This equation does not take into account the frictional forces on the surfaces between the rotating nacelle and the oil embedded bearing and are assumed to be negligible. The usefulness of equation (1) is that it would demonstrate whether a certain motor has the input torque needed to yaw at a practical rate. In addition, one can play with the gear ratios and determine how the acceleration of the nacelle would be affected. Ultimately, a quick acceleration to the specification yaw rate is desired in order to react quickly to varying wind directions. With this in consideration as well as sizing constraints, an 84-tooth sun gear and 30 tooth motor gear were chosen and are driven by a 3V stepper motor with a max holding torque of 0.48 Nm. Table 4 demonstrates a sample calculation created in Excel.

Table 4. Gear Calculations

Gear Calculator [units in m]					
No.	Item	Symbol	Formula	Planet (1)	Sun (2)
1	Module	m	Set Value	1	
2	Reference Pressure Angle	α		20	
3	Number of Teeth	z		30	84
4	Center Distance	a	NOTE1 $\frac{(z_1+z_2)m}{2}$	0.0570	
5	Reference Diameter	d	zm	0.03	0.084
6	Base Diameter	d_b	d cos α	0.0281908	0.0789342
7	Addendum	h_a	1.00m	1	1
8	Tip Diameter	d_a	d + 2m	0.032	0.086
9	Root Diameter	d_f	d – 2.5m	0.0275	0.0815

Acceleration Calculator		
Motor Torque	0.1	N*m
Planet Gear Mass	0.3	kg
Nacelle+Rotor Mass	4	kg
Nacelle Length	0.24	m
Nacelle Width	0.175	m
Planet Moment of Inertia	3.38E-05	kg *m^2
Nacelle Moment of Inertia	2.94E-02	kg*m^2
Acceleration (Nacelle)	12.7	rad/s^2
Acceleration (Planet)	48.3	rad/s^2
Time, 0 - π(rad/s)	0.247	sec

The remaining analyses are stress analyses performed on the various materials making up the yaw system and base structure. An additional specification needed to be met. Specification A states that the turbine must withstand continuous wind speeds of up to 18 m/s. As a result, any simulation or analysis performed was done using a wind speed of 18 m/s. Furthermore, the need for a wire passage through the center of the turbine imposed an additional specification of the turbine design and became one of the driving dimensions.

First, a stress analysis was done on the rotating shaft and then the tower. Figure 8 shows the forces that were considered in the analysis. The shearing force, V, is a combination of the drag force from the nacelle casing and the thrust produced by the blades. The drag force was estimated by performing a SolidWorks flow simulation over the casing. Table 5 displays the output values of this simulation. Thrust produced by the blades was estimated using Blade Element Momentum theory using MATLAB. The moment M_g is a result from the gyroscopic effects. All other forces shown are reaction forces.

Table 5. SolidWorks Values

Goal Name	Unit	Value	Averaged Value	Minimum Value	Maximum Value
GG Force (X) 1	[N]	11.13541279	11.13527538	11.1297837	11.14796008

For this particular part, a normal bending stress and shear stress analysis were performed. A design factor of 2.0 was designated and used to determine a maximum inner diameter that would satisfy stress requirements using 6061 aluminum. Table 6 display the calculations and the factor of safety of 12.0 with the chosen inner diameter.

Table 6. Rotary Shaft Stress Calculations

Rotary Shaft Stress Analysis		
Normal Bending Stress		
Material:	6061 Aluminum	
Yield Strength	276	Mpa
Design Factor, n_d	2	
σ_allowable	138	MPa
Moment due to Gyroscopic Effects:		
Rotor Mass	1	kg
Rotor radius, r	0.2286	m
ω_rotor	5000	RPM
ω_yaw	3.141592654	rad/s
Mass Mom. of Inertia	0.02612898	kg*m^2
M_o	42.98	Nm
D, Outer Diam.	0.035	m
d, max. inner diam.	0.0343	m
	34.33	mm

Calculating Factor of Safety		
Bending Stress		
M_o	42.98	Nm
D	0.035	m
d, chosen inner diam.	0.02	m
σ	1.14E+07	Pa
Allowable Stress	1.38E+08	Pa
Factor of safety	12.07	
Shear Stress		
V	27.7	N
Shear Stress	85499.96458	Pa
Allowable Stress	6.90E+07	Pa
Factor of safety	403.5	

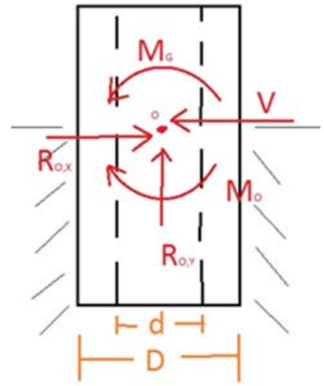

Figure 8. Rotary Shaft FBD

Analysis was then done on the tower. The following FBD, Figure 9, shows which forces were considered in this analysis. F_D is the force due to drag of the nacelle casing, M_g is the moment due to gyroscopic effects, F_D_tower is the drag force of the tower, and F_T is the thrust produced by the blades. Again, the drag force of the tower was estimated using a SolidWorks flow simulation. A normal bending stress analysis was then performed. Since the tower and rotating shaft have the same cross sections the bending stress equations are the same. For design a design factor of 2.0 was specified and the final factor of safety was calculated to be 22.6. Table 7 display the calculations performed in Excel.

Table 7. Tower Stress Calculations

Tower Bending Stress Analysis		
Material:	1026 Steel CD	
Yield Strength	415	Mpa
Design Factor	2	
σ_allowable	207.5	MPa
Tower height, l	0.548	m
Tower Drag Force	11.02	N
Torque due to Gyroscopic Effects:		
Rotor Mass	1	kg
Radius, r	0.2413	m
ω_rotor	5000	RPM
ω_yaw	3.141592654	rad/s
Mass Mom. of Inertia	0.029112845	kg*m^2
M_g	47.88871052	Nm
Nacelle Drag Force	11.14	N
Rotor Thrust Force	16.56	N
Hub Height, h	0.6	m
M_a	66.94891052	Nm
D, outer diam.	0.0508	m
d, max. inner diam.	0.050478588	m
	50.47858811	mm

Rotary Shaft Stress Analysis		
Shear Stress in Bending		
Design factor, n_d	2	
τ_allowable	69	Mpa
Nacelle Drag Force	11.14	N
Rotor Thrust Force	16.56	N
Shear Force, V	27.7	N
D, outer diam.	0.035	m
d, max. inner diam.	0.03499	m
	34.9854	mm
Calculated Factor of Safety		
M_a	66.95	Nm
D, Out Diam	0.0508	m
d, inner diam.	0.0412	m
σ	9.17E+06	Pa
σ_allowable	2.08E+08	Pa
Factor of Safety	22.6	

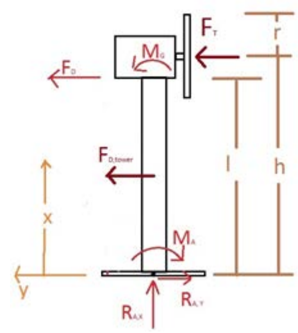

Figure 9. Tower FBD

Yaw System Testing:

During the design of the turbine and the yaw system it became apparent that a device would need to be fabricated that will test the yaw system prior to the competition. The solution to this was to create a turntable that would replicate the one that will be used at competition. Based off the rules for this year's contest the designed turntable must rotate from 0 to 30 rpm both clockwise and counterclockwise. The turntable base plate was also designed to exactly match the one that will be used at competition to provide the most accurate testing environment.

The turntable design that was chosen was a design that utilized a sprocket gear and roller chain to turn the base plate that the turbine was mounted too. A servo motor that rotates at 55,000 rpm, and has a planetary gear assembly mounted on it to slow the rotation down to 40 rpm, was used to rotate the turntable. This type of motor was used because it is able to provide a lot of torque while being cheap and reliable. The large amount of torque is needed to rotate the turbine because of the many forces that are acting on it like the weight as well as the forces from the turbine spinning off axis in the wind. A potentiometer will be used to control the rotational speed of the turntable to increasing in resistance to slow the table. A set of switches will be used to switch the rotation direction of the turntable by reversing the current through the motor. When the current is reversed, the motor will spin in the opposite direction allowing us to rotate the device clockwise and counterclockwise.

Aerodynamic Consideration:

The flow analysis shown in Figure 10 was calculated to show the wake effects and drag effects on the nacelle of the turbine. These simulations were also used to determine the placement of the rotary encoder. The vane design was altered to evenly distribute the weight which would allow for a more fluid rotation of the encoder.

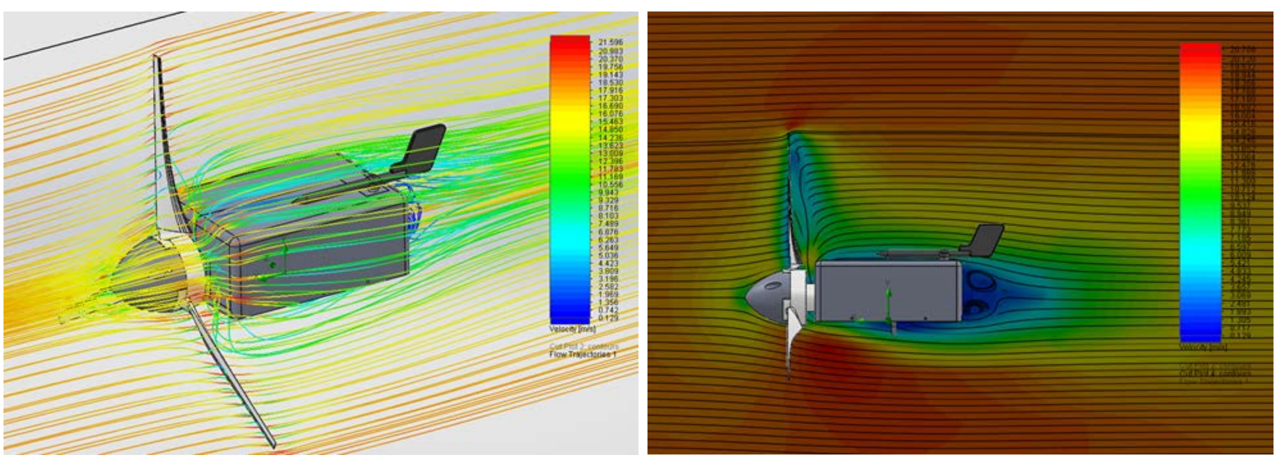

Figure 10. Airflow Analysis of Turbine

Electrical Design:

The electrical system is designed to convert the mechanical energy from the wind to electrical energy to power the load. The block diagram shown in Figure 11 describes the process of how the electrical system works.

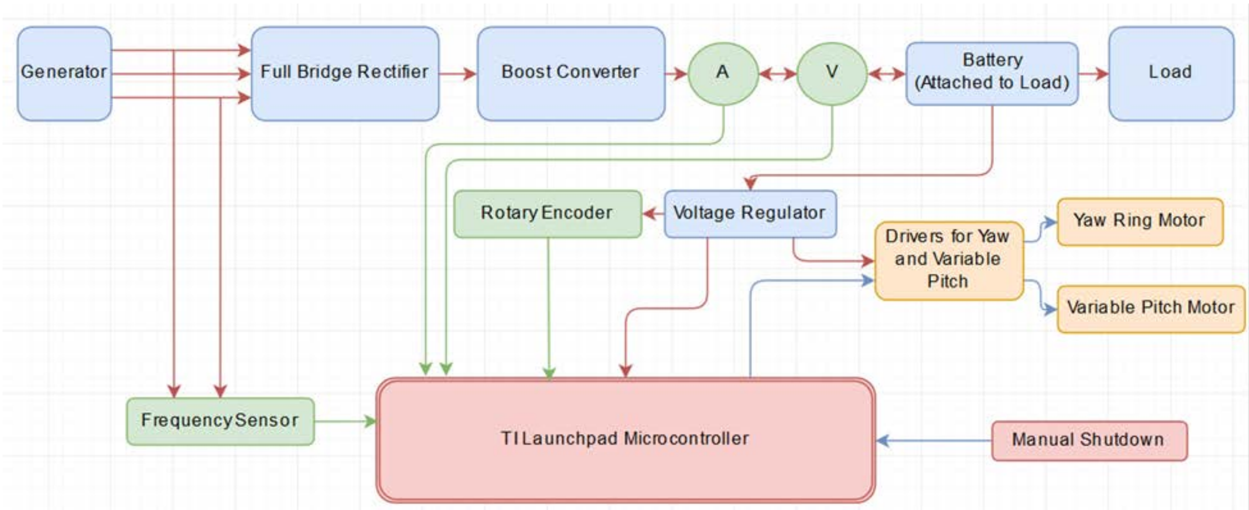

Figure 11. Electrical Block Diagram

Three Phase Generator:

The three-phase generator is an Ammo 3600 in-runner brushless permanent magnet synchronous generator. This motor was chosen for its low cogging torque, known voltage and current characteristics, as well as its efficiency. The generator has a cogging torque of approximately 4 mNm. Which allows for a lower cut-in speed for the turbine. This generator will produce 1V at approximately 1800 RPM and can handle a maximum current of 50A. This current rating far exceeds the maximum current necessary for scale performance, which peaks at approximately 4A. The generator outputs power in a 3-phase system, which allows a higher generator efficiency of up to 89%. The LTSpice model seen in Figure 12 was used to model the generator. The model was fully parameterized based on the wind speed, V, and as well as the open circuit voltage of the motor, VOPEN. The

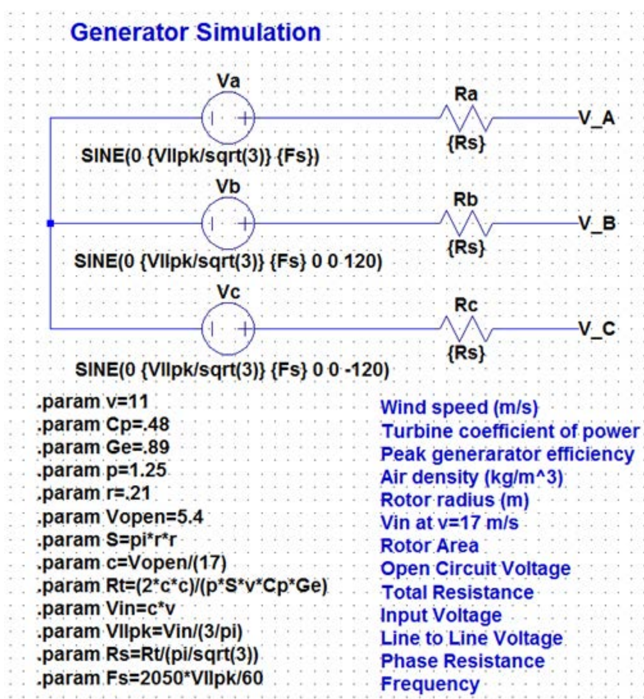

Figure 12. Generator Simulation

internal resistance of the generator is modeled by RS.

Full Bridge Rectifier:

The full bridge rectifier is used to convert the three-phase signal from the generator to a DC signal. It operates by connecting each of the phases to the anode of one power diode and the cathode of another. Each set of diodes are put in parallel with the other sets of diodes which are all configured in a similar manner. The schematic of this full bridge rectifier can be seen in Figure 13. This rectifier is the first section of the primary power path. Due to this, a low activation voltage was needed in the diodes to minimize the power lost in the conversion. The Vishay VS-STPS20L15DPBF were chosen to comprise the 3-phase rectifier for this reason. These diodes have a forward voltage drop of 300mV at 3 amps, the current expected at maximum wind speed. Aluminum heat sinks were affixed to these devices in order to dissipate the lost power as heat. The DC output of the bridge rectifier has a 1mF aluminum capacitor in order to provide voltage smoothing.

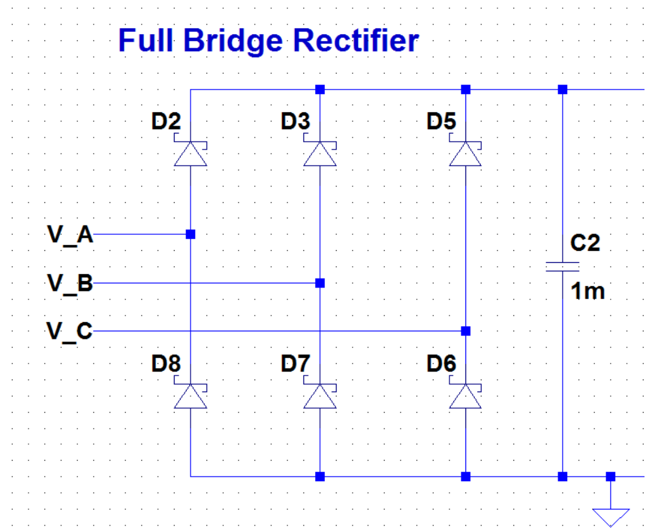

Figure 13. Full Bridge Rectifier

Boost Converter:

The boost converter converts the DC voltage from the full bridge rectifier to a higher DC voltage for the load. It is comprised of an inductor, low-side NMOS, high side PMOS, and a Schottky diode. The boost converter works by switching the NMOS to draw current from the inductor. When the NMOS is switched on, high current is drawn through the low resistance of the device. The NMOS is then switched off, forcing the inductor to continuously conduct high current, but instead, force it through the diode and PMOS in parallel. After the NMOS is switched off, The PMOS is switched on at the correct time in order to provide a low resistance path for the current to flow. To keep the system in continuous current conduction mode the inductor needed to be 20uH or higher. If it was below this amount the current would tend to zero every switching period and no boosting would occur. How the timing was achieved is in the gate driver section. When both

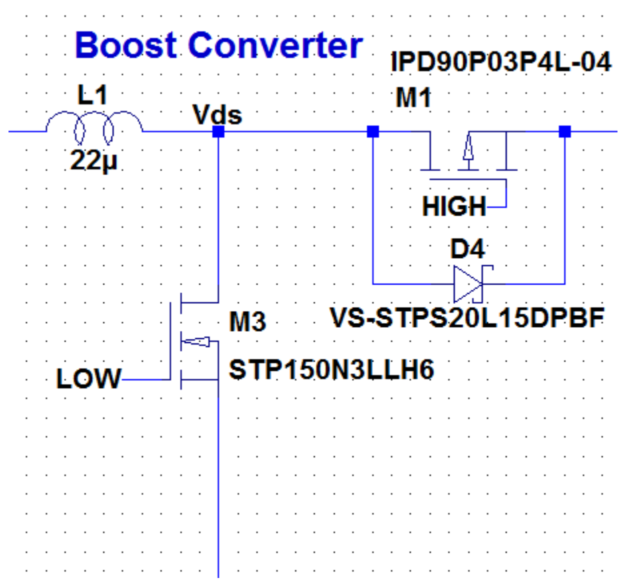

Figure 14. Boost Converter

the NMOS and PMOS are switched off, the current is allowed to flow into the load via the Schottky diode in order to ensure that breakdown voltages of either MOSFET are reached. All 4 devices were chosen for their power and efficiency characteristics. The schematic for this sub circuit can be seen below in Figure 14. The inductor, TT Electronics HA55L-3623220LF, was chosen for its high saturation current of 26A and low resistance, 3.35 mΩ. The low side NMOS, STMicroelectronics STP150N3LLH6, was chosen for its low on-state resistance of 3.5 mΩ. The high-side PMOS, Infineon Technologies IPD90P03P4L-04, was chosen for its low on-state resistance of 4.1 mΩ as well. The Schottky diode is the same diode chosen in the 3-phase rectifier.

Microcontroller:

The microcontroller is the Texas instruments Launchpad model MSP430F5529. This microcontroller is used for low power applications and is responsible for the control loops and power regulation. The microcontroller is connected to the wind turbine through a 40 pin header on the power electronics board. The MSP4305529 microprocessor and the associated development board were chosen for the following reasons:

- The processor is designed for ultra-low power application, offering a variety of low power and sleep modes.
- The development board has an integrated Universal Serial Bus (USB) hub and debug module, which can be disabled via jumpers when not in use which will cause a reduction in power demands.
- The microprocessor has an integrated multi-channel 12-bit analog to digital converter (ADC). The ADC is used to measure voltages that are directly proportional to the output current as well as the output voltage.
- The microprocessor has an integrated comparator. The comparator is used for level crossing detection along with one of the timers to sense the frequency.
- The microprocessor has four 16 bit timers. The timers are used in the design to determine the frequency, apply averaging, and wake up the processor as necessary.
- The microprocessor able to run up to 25 MHz and has a fast wake-up features.

Power Management:

Power for the components is powered through a buck converter IC and voltage regulators. The IC can be configured to regulate the output voltage at a certain point. This will ensure that minimal power is being consumed from the components. The voltage regulator is DC-DC buck-boost voltage regulator, the Linear Technologies LTC3127, which was chosen for its wide range of voltage inputs. The switching circuit, Linear Technologies LTC4415, was chosen for its ideal diode characteristics. In previous years, a super capacitor was used to ensure that there was continual power supplied to this system. However, since a new rule change has been added this supercapacitor has been removed from the design and a battery has been attached to the load to power the system.

Current Sensor:

The current sensor used is the HO-P/SP33 series current transducer. This will let the current flow through it and output a reference voltage. This reference voltage will be fed into one of the analog to digital converter pins on the microprocessor which will tell us the output current after dividing by the current sensors resistance.

Voltage Sensor:

The voltage sensor is a basic voltage divider with a TI LMV822 op amp at the end. The resistors and filter capacitor values were chosen such that the output voltage from this sensor will all be one fifth of the input voltage. Feeding this voltage into one of the analog to digital converter pins on the microcontroller the output voltage can be easily calculated.

Frequency Sensor:

The frequency sensor is a two part schmitt trigger. The first is a differential amplifier which is referenced to two phases of the generator. This will combine the two different phases into one phase and send the output to a TI SN74LVC2G14 which is a schmitt trigger that will convert the sine wave from the inputs into a square wave for the microprocessor to easily calculate the frequency.

Gate Drivers:

The gate driver circuit uses digital logic and bootstrapped gate drivers to quickly and safely switch the MOSFETs in the synchronous boost converter. The driver of this board is the clock signal from the microcontroller. This is set at a 8 kHz switching frequency by default and can vary depending on the power output. To ensure an accurate output, the outputs are crossed into two logic gate inputs. This is to ensure that only one MOSFET is on at a time. Load overvoltage is also implemented into the logic. This is accomplished through a voltage divider inputted into one of the logic gates. This will prevent the NMOS in the boost converter from switching, reducing the output voltage. This has been implemented to protect the load from too high of voltages.

Yaw Ring:

The electrical design of the yaw ring is dependent on using a rotary encoder, a 3D printed fin and a stepper motor. The stepper motor is controlled by a microcontroller and the direction of the step is determined by a wind vane. The wind vane will be created using a quadrature rotary encoder, EN14 by Bourn Inc, attached to a 3D printed fin. Depending on the wind direction, the wind vane will sense the direction and trigger one or several of its 64 pulses and send the information to the decoder chip. This chip, ELM404DS, will interpret the direction of the encoder and send a positive or negative pulse to the microprocessor. Figure 16, shows the graphical representation of yaw system control system design.

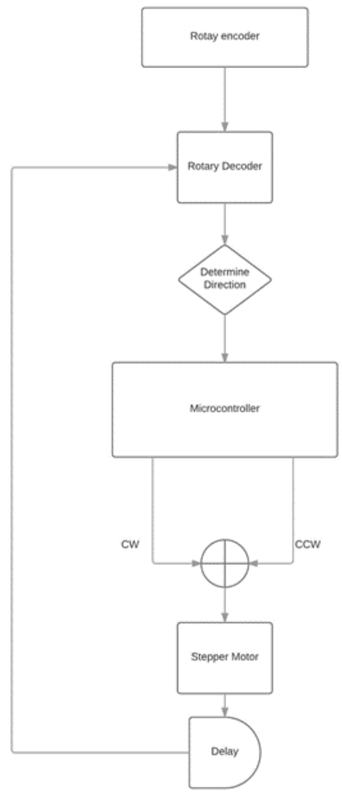

Figure 16. Yaw Ring Diagram

Maximum Power Tracking:

The control system uses a hill climbing maximum power point tracking algorithm to determine the optimum boost converter duty cycle. The algorithm adjusts the duty cycle up or down while monitoring the output power then determines whether to maintain the direction of change or go the opposite direction based on the sampled output current. For a given wind speed, there is an optimal duty cycle that delivers the most output power. This control system is represented graphically in Figure 15.

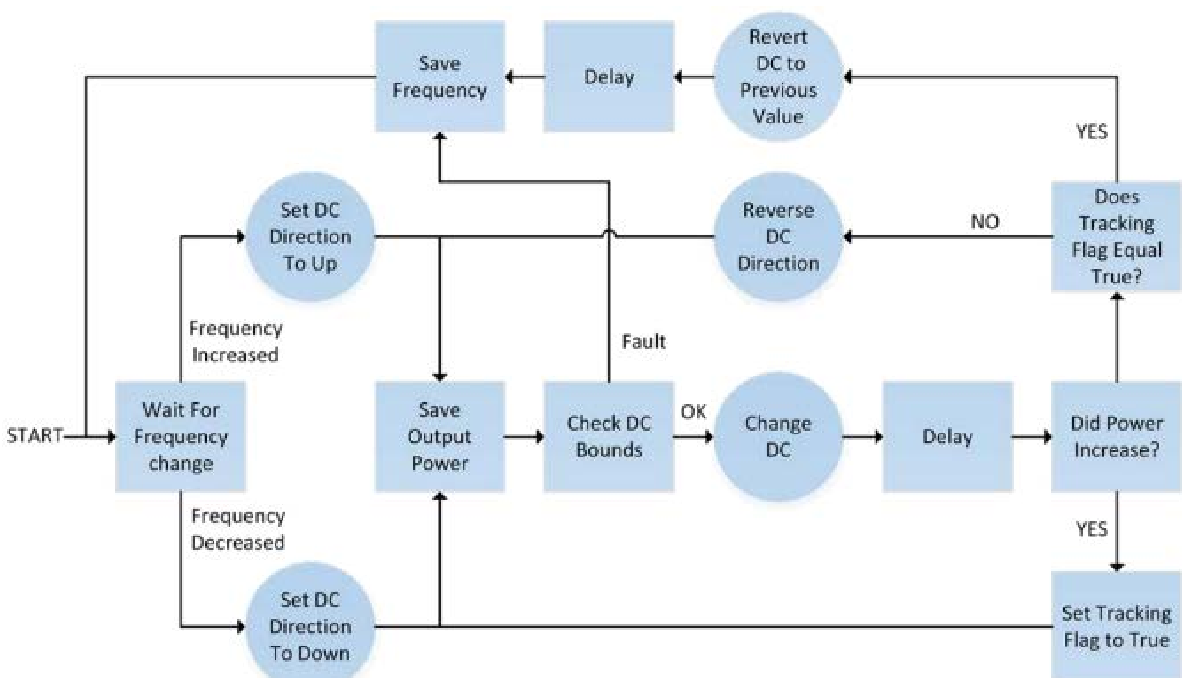

Figure 15. Power Tracking Diagram

Braking with Variable Pitch:

The electrical design of the variable pitch will use the frequency, voltage and current sensors, and a stepper motor. Initially the turbine blades will be fully feathered, producing no lift. Once the turbine has been connected to the load, the battery attached to the load will power the stepper motor and the microcontroller in the nacelle, which will push the blades forward. This will begin generating lift and producing power in the system. If, at any time, the load is disconnected, or the emergency stop is signaled the stepper motor will shut down allowing the spring attached to the variable pitch shaft to force the blades back to the fully feathered position. If the wind speed increases to 18m/s or higher the system will undergo the same process only the blades will feather halfway which will reduce the lift slowing the rpm considerably. The blades will stay this way for two minutes then return to the frontal position and the cycle repeats.

Printed PCB:

The printed circuit board (PCB) was designed for ideal signal integrity. The input and output terminals were placed close together and bypass capacitors were placed at many locations to reduce noise in the signals. The MOSFET driver was placed as close to the power MOSFETS as possible to provide an optimal ground path. Since the generator could have an output current of eighteen amps' trace widths of 300mil were used to prevent destruction of the system. Routes on the ground plane were minimized as much as possible to provide for good signal integrity.

Load:

The simulation for the load can be seen in Figure 17. This load system will comprise of a battery, a voltage sensor, current sensor and two relays, all attached to a pump. This system is built to help power the turbine at startup without wasting any power to the load. This will allow a microprocessor to know the power leaving, and coming into the load and switch the relays as needed. This will switch off the battery and switch on the load. A capacitor is added to the system to help make the transition between the battery and the load smoother. Once the current drops below a certain point the microprocessor will switch the two relays allowing the battery to repower the load. The pump in the load system will be attached to a water cooling system that is designed to remove the heat generated by our components to keep them from overheating.

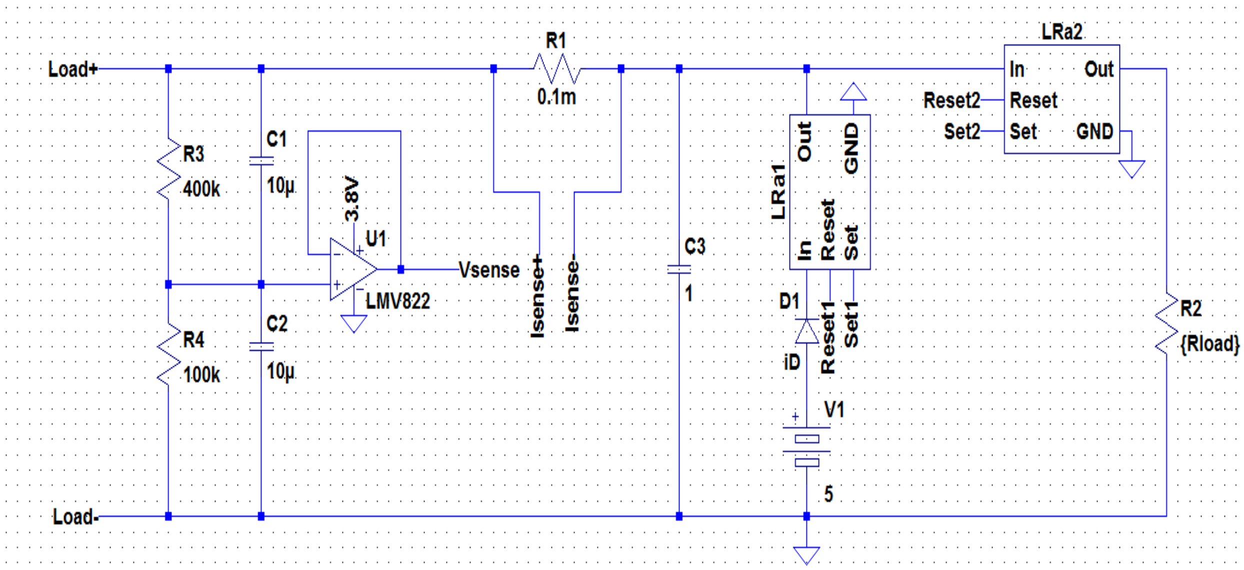

Figure 17. Load Simulation

Software:

Many different software's were used for this project. On the electrical side of this project LTSpice, and Eagle Cadsoft were used to design, simulate, and build the power circuit board. The control system used Texas Instrument's Energia programming software to implement the control loops in the microcontroller. On the mechanical side, SolidWorks was used to design and simulate mechanical components of the wind turbine and MATLAB was used to further analysis components.

Appendix I – Matlab Calculations:

Blade Geometry

```
R=8; %Inches
r=linspace(0.1,1,9)*R;
%Given Information
rl=0.*r;
c=R*[0.191 .159 .128 .105 .088 .076 .067 .059 .053];
phi=[32 22.5 17.0 13.5 11.2 9.6 8.4 7.4 6.6];
alpha=0;
theta_p=phi-alpha;
for n=1:9
    %Data Points for Trailing Edge
    trailing_x(n)=c(n)*cosd(theta_p(n));
    trailing_y(n)=c(n)*sind(theta_p(n));
    %Data Points for Leading edge
    lead_x(n)=0;
    lead_y(n)=0;
end
%Plot Function For Blade Geometry
figure
plot3(trailing_x,trailing_y,r)
hold on
plot3(lead_x,lead_y,r)
xlabel('x')
ylabel('y')
zlabel('r')
xlim([0 8])
ylim([0 8])
hold off
```

Stress Analysis

```
w=2/16;                 %pounds
t=linspace(0.4,0.1,9);  %inches
g=32.2;                 %in/s^2
omegaRPM=3000;          %rpm (Estimate based off of
previous year)
omega=omegaRPM*(2*pi)/60;  %rad/s
Ac=c.*t;                %inches^2
ut=6650;                %psi
q=2*pi;                 %rad/s
I=c.*power(t,3)/12;     %moment of inerita
J=(1/12).*(c.*t).*...
    (power(c,2)+power(t,2));%polar moment of inertia
%stresses on blade at sections
%Gravity Stress
sigGravity=w.*r./(t.*power(c,2)/6)  %psi
%Centrifugal Stress
fc=(w/g).*r./12*power(omega,2);
sigC=fc./Ac             %psi
%Yaw Stresses
mYaw=-2*q*omega*I;
tauYaw=abs(mYaw.*(c./2)./J)     %psi
%Plot Figure for Blade Stresses
figure
hold on
plot(r,sigC,'r')
plot(r,sigGravity,'--g')
plot(r,tauYaw,'.-b')
legend('SigC','SigGravity','TauYaw')
xlabel('Radius (In)')
ylabel('Stress (psi)')
title('Summary of Stresses')
sigGravity =
  Columns 1 through 7
        0.6425    2.1738    5.7220   12.9400   26.6335
50.6024   92.4880
  Columns 8 through 9
  173.8333  333.7487
sigC =
   1.0e+03 *
  Columns 1 through 7
    0.0418    0.1177    0.2494    0.4627    0.7982    1.3097
2.1104
  Columns 8 through 9
        3.4929    6.0242
tauYaw =
  Columns 1 through 7
  193.4373  188.6019  184.9758  173.8671  155.6173  130.6445
101.9181
  Columns 8 through 9
   72.8816   44.1016
```

Published with MATLAB® R2016a

Flow Conditions and Forces solution for CWC_LS Blade

```
%This is an interative solution using strip theory (Momentum
theory
% blade element theory) solving for the induction factors a, a', Cl,
Ct,
% and finally calculating the thrust force of the rotor. For a
detailed
% description of the process refer to page 136 in "Wind Energy
Explained"
% Strip Theory (including wake rotation)
% Assumptions:
% - Negligible drag thus Cd = 0
% - No tip losses for a < 0.5, Ct < 0.96
% - Since drag is neglected then the thrust force is equal to the
normal
% component of the lift force
% NOTE - since only 9 sections of the airfoil are known it is
assumed that
% the calculated induction factors and coefficients represent their
entire
% element of the airfoil
% Define variables
B = 3;                  %Blade number
u_inf = 18;             %Upstream velocity [m/s]
pitching = 10;      %Additional pitching angle of blades [degrees]
```

```
omega = 472.4;          %Rotor Angular velocity [rad/s]
r = 9:-0.9:1.8;         %Intermediate radius [in]
R = 9;                  %Rotor radius [in]
for tsr = 1:20          %Tip speed ratio
        tsr_r = r.*tsr / R ;    %Relative tip speed ratio
        dr = 0.9;               % radial element size[in]
        Cd=0.001;
        rho = 1.225;            %Air Density [kg/m^3]
        %Section Blade Pitch angle [degrees]
        standard_pitch = [6.4 7.4 8.4 9.6 11.2 13.5 17 22.5 32];
        %Section Blade Pitch angle (Angle between chord and
rotation plane) [rad]
        theta_p = (pi/180)*(standard_pitch + pitching);
        c = [.42 0.47 0.54 0.61 0.7 0.84 1.02 1.27 1.53];
%Chord [in]
        sldty = (c.*B)./(r.*2*pi);                  %Solidity
[unitless]
        % INITIAL GUESS
        a = 3/8*ones([1,numel(r)]);
        a_pri = (1-3*a)./(4*a-1);
        %phi=[32 22.5 17.0 13.5 11.2 9.6 8.4 7.4 6.6];
        %Iterations to convergence
        iter = ones([1,numel(r)]);
        tol = 1e-03;            % tolerance of solution
        err = ones([1,numel(r)]);
        for i = 1:numel(r)
        while err(i) > tol
        %Angle of the relative wind
        phi(i) = atan( (1-a(i)) / ( (1+a_pri(i))*tsr_r(i)) );
        %Angle of attack [deg}
        attack(i) = (180/pi)*(phi(i) - theta_p(i));
        %Lift Coefficient
        Cl(i) = ( 4*sin(phi(i))/sldty(i) ) * (cos(phi(i)) - tsr_r(i)...
        *sin(phi(i))) * (sin(phi(i)) + tsr_r(i) * cos(phi(i)))^(-1);
        %Thrust Coefficient
            Ct(i) = sldty(i) * (1-a(i))^2 * (Cl(i) * cos(phi(i)) * ...
        (1/(sin(phi(i))^2));
        %Determine whether rotor is in turbulent wake state
(a > 0.5) for
        %which then the simple theory would not be valid
        if Ct(i) > 0.96
        %Correction Factor
        F = (2/pi)*acos(exp(-(((B/2)*(1-r(i)/R))/...
        (r(i)*sin(phi(i))/R))));
        %Improved induction factor
        a_new = (1/F)*(0.143 + sqrt(0.0203 - 0.6427*...
        (0.889 - Ct(i))));
        %Improved Angular induction Factor
        a_pri_new = ( ((4*F*cos(phi(i))) / ...
        (sldty(i)*Cl(i))) - 1)^(-1);
        else
        %Improved Induction factor
        a_new = ( (1 + (4*(sin(phi(i))^2)) / (sldty(i)*Cl(i)*...
        cos(phi(i)))))^(-1);
        %Improved angular induction factor
        a_pri_new = (( (4*cos(phi(i))) /...
        ( sldty(i)*Cl(i)) ) - 1)^(-1);
        end
        % The error between guess and improved value
        err(i) = abs(a(i) - a_new);
        a(i) = a_new;
        a_pri(i) = a_pri_new;
        iter(i) = iter(i) + 1;
        end
        end
        %Force Calculations
        % Here only blade element theory is used (eqn 3.80 pg.
125
        %Inner elements
        dFt = sldty.*pi.*rho.*(((sin(phi)).^2).^-
1).*(u_inf^2).*((1-a).^2).*...
    Cl.*cos(phi).*r.*dr.*(1/39.3701)^2;
        %Outer elements
        dFt(1) = dFt(1)/2;
        dFt(end) = dFt(end)/2;
        %Total Thrust Force
        thrust(tsr) = sum(dFt);
        %Solve Cp Values
  first=(16/27)*tsr*power(tsr+((1.32+power((tsr-8)...
        /20,2)/power(B,2/3))),-1);
  second=(0.57*power(tsr,2))/((mean(Cl)/Cd)*(tsr+(1/(2*B))));
        Cp(tsr)=first-second;
        llambda(tsr)=tsr;
        %Angle of Attack
        for x=1:9
        phiD=phi.*180/pi;
  angleAttackSec(tsr,x)=phiD(x)-standard_pitch(x);
        end
        %Average Ange of Attack Per Blade
        angleAttack(tsr)=mean(angleAttackSec(tsr,:));
        betsLimit(tsr)=16/27;
end
%Plot Cp vs Llambda
plot(llambda,Cp,'-o')
hold on
plot(llambda,betsLimit,'--r')
xlabel('Llambda')
ylabel('Cp')
legend('Calculated Values','Bets Limit (0.593)')
ylim([0 0.6])
grid
title('Cp vs Llambda')
hold off
```

Published with MATLAB® R2016a

Appendix II - References:

J. F. Manwell, J. G. McGowan, and A. L. Rogers, *Wind energy explained: theory, design and application*. Chichester, U.K.: John Wiley & Sons, Ltd., 2011.

"NASA/LANGLEY LS(1)-0417 (GA(W)-1) AIRFOIL (ls417-il)," *NASA/LANGLEY LS(1)-0417 (GA(W)-1) AIRFOIL (ls417-il)*. [Online]. Available: http://airfoiltools.com/airfoil/details?airfoil=ls417-il. [Accessed: 31-Mar-2017].

Appendix III - PCB One Line Diagram: